Trigger simulation study of the air shower fluorescence telescope FAMOUS

von

Dominik Sommer

Bachelorarbeit in Physik

vorgelegt der
Fakultät für Mathematik, Informatik und Naturwissenschaften
der
Rheinisch Westfälischen Technischen Hochschule Aachen

im November 2014

angefertigt am

III. Physikalischen Institut A

Erstgutachter und Betreuer

Prof. Dr. Thomas Hebbeker
III. Physikalisches Institut A
RWTH Aachen

Zweitgutachter

Prof. Dr. Martin Erdmann
III. Physikalisches Institut A
RWTH Aachen

Contents

1. Outline

Cosmic ray particles entering the atmosphere of the Earth interact with the air particles causing so-called extensive air showers of secondary accelerated particles. The Pierre Auger Observatory in Argentina is the world's largest observatory researching these showers. Therefore, a hybrid detector consisting of a surface detector (SD) and a fluorescence detector (FD) is used. The surface detector consists of 1600 water Cherenkov stations and measures the lateral shower profile at ground level. The fluorescence telescopes use conventional photo-multiplier tubes to detect the fluorescence light emitted by the shower and measures the longitudinal shower profile. FAMOUS (**F**irst **A**uger **M**ulti-pixel-photon-counter-camera for the **O**bservation of **U**ltra-high-energy-cosmic-ray air **S**howers) is a 64 pixel fluorescence detector which uses silicon photomultipliers (SiPMs) to detect the fluorescence light emitted by extensive air showers. At the moment a 7 pixel prototype is tested in Aachen. In this thesis a trigger algorithm for the 64 pixel version of FAMOUS and the reconstruction of the shower geometry is discussed based on simulated data. The simulated data is created by the use of simulation frameworks CONEX, a simulation program for high energy extensive air showers, Auger Offline for the simulation of fluorescence light and Geant4 for the simulation of the optical system and the SiPMs of the FAMOUS telescope. Finally an outlook on furher improvements will be given.

2. Cosmic rays

Radioactivity was discovered 1896 by Henri Becquerel [1]. Until 1912 it was scientific consensus that the ionisation of the air measured on the surface of the Earth was caused by radioactive elements in the Earth or the air. 1912 Victor Hess discovered that ionisation decreased up to a height of 1 km but increased from there on and therefore concluded that this kind of radiation enters the atmosphere from above [2].

2.1 Energy spectrum

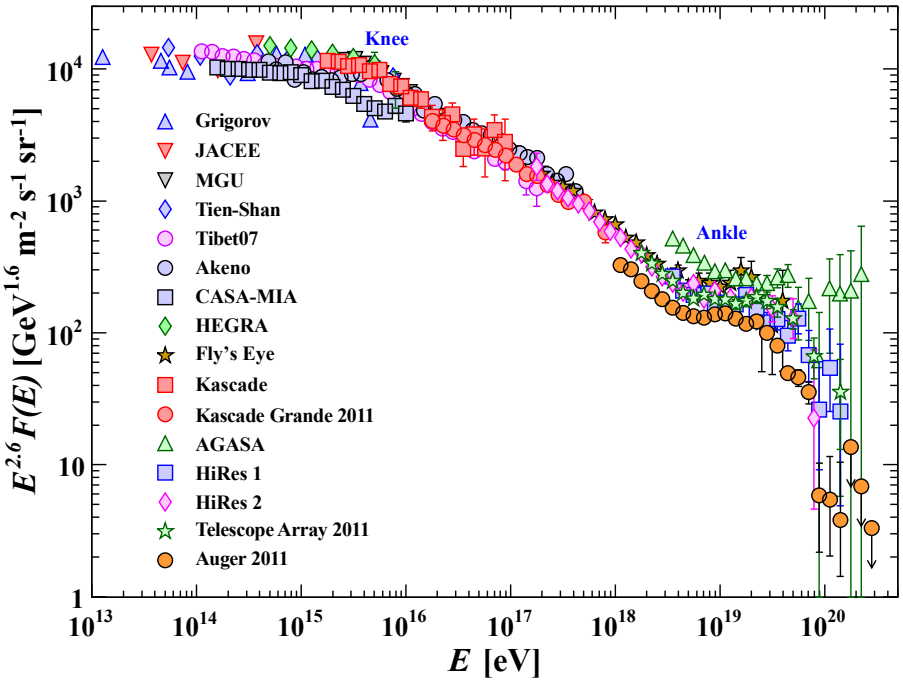

Figure 2.1: Energy spectrum of all cosmic rays measured by indirect detection methodes. Taken from [3].

In figure 2.1 the flux of cosmic rays is shown multiplied with the energy to the power of 2.6, to reveal the structure. It can be seen that the flux follows a power law

$$\frac{dN}{dE} \propto E^{\gamma} \tag{2.1}$$

For low energies the flux falls with $\gamma = -2.7$. At $5 \cdot 10^{15}$ eV, commonly referred to as knee, γ changes to -3.1. A further steepening called the second knee occurs at energies of $4 \cdot 10^{17}$ eV.

At the so-called ankle at energies of $5 \cdot 10^{18}$ eV, the flux flattens to $\gamma = -2.6$. Finally at what is to be believed the GZK-cutoff for energies of above 10^{20} eV the flux rapidly falls to zero. This energy distribution of cosmic rays leads to the very rare ultra high energy cosmic rays (UHECRs). Cosmic rays with an energy of 10^{19} eV have an estimated arrival rate of 2 per square kilometre per year [4]. Increasing the energy to 10^{20} eV this arrival rate decreases roughly with a factor of 100 so that huge experiments such as the Pierre Auger Observatory with a detector area of more than 3000 km^2 are needed to investigate UHECRs with sufficient statistics.

2.2 Extensive air showers

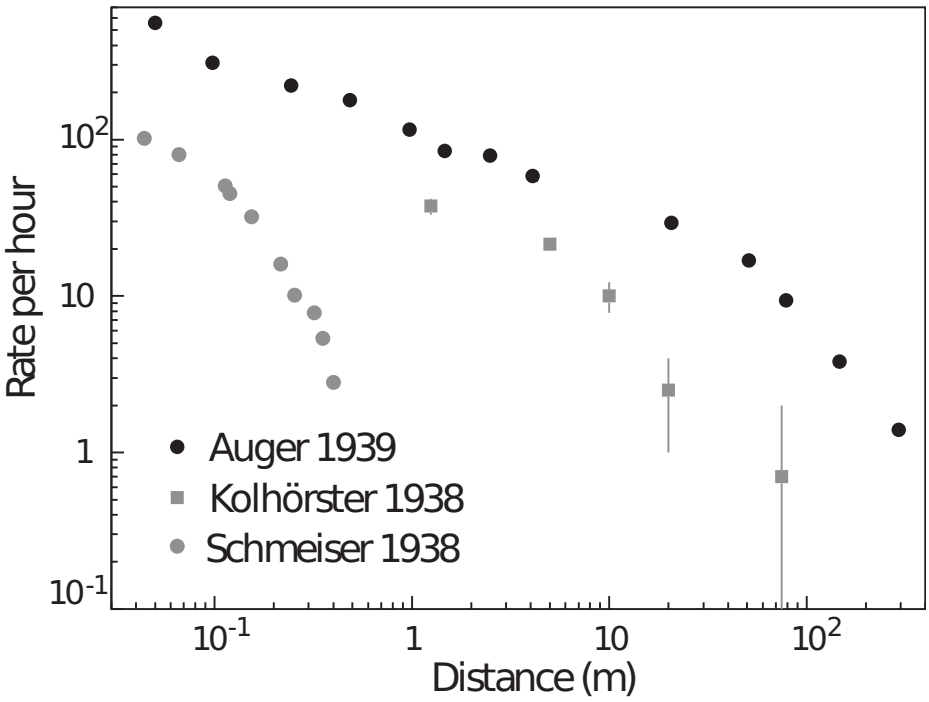

Figure 2.2: Decoherence curves measured with Geiger counters. The differences in coincidence rates of the three groups are caused by different effective Geiger counter areas (Auger: 200 cm^2, Kolhörsters: 430 cm^2 and Schmeiser: 91 cm^2) and the different altitudes at which the measurements were performed (Auger: 3450 m, Kolhörsters and Schmeiser: 0 m) [5].

In 1934 Bruno Rossi recognised that particles arrived simultaneously at detectors separated from each other and therefore postulated air showers [5]. However he had to leave Italy soon after and could not follow up his work. In 1938 the two German groups arround Schmeiser and Kolhörster not knowing

about Rossi's work measured the rate of coincidences depending on the distance between two detectors. Figure 2.2 shows the measured decoherence curves of Schmeiser, Kolhörster and Auger. In 1939 Auger and his collaborators found that the coincidence rate of two distant counters greatly exceeded the rate of randomly coincident counts and estimated the energy of some primary particles to be arround 10^{15} eV by examining the total number of particles in the shower.

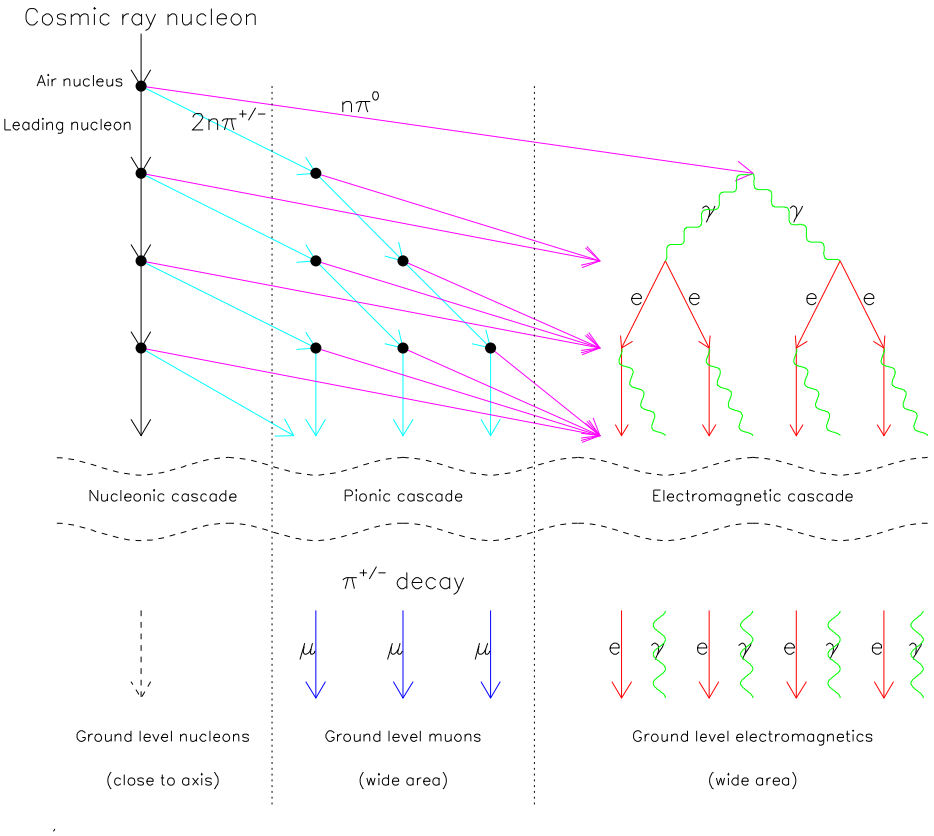

Figure 2.3: Sketch of a cosmic shower showing the hadronic, myonic and electromagnetic component. Most important for the detection of fluorescence light is the electromagnetic component, since it contains a large number of low energy particles that can excite air molecules such as nitrogen which emit the fluorescence light when they decay [6].

As described above primary particles striking the atmosphere of the Earth interact with air molecules, mainly nitogen and oxygen. Thereby various secondary particles are created and interact themselves with air particles or decay leading to a cascade of particles. As shown in figure 2.3 this so called shower consists of a myonic, a hadronic and an electromagnetic component. Figure 2.4 shows the longitudinal profile of the energy deposition of a shower measured by the Pierre Auger Observatory.

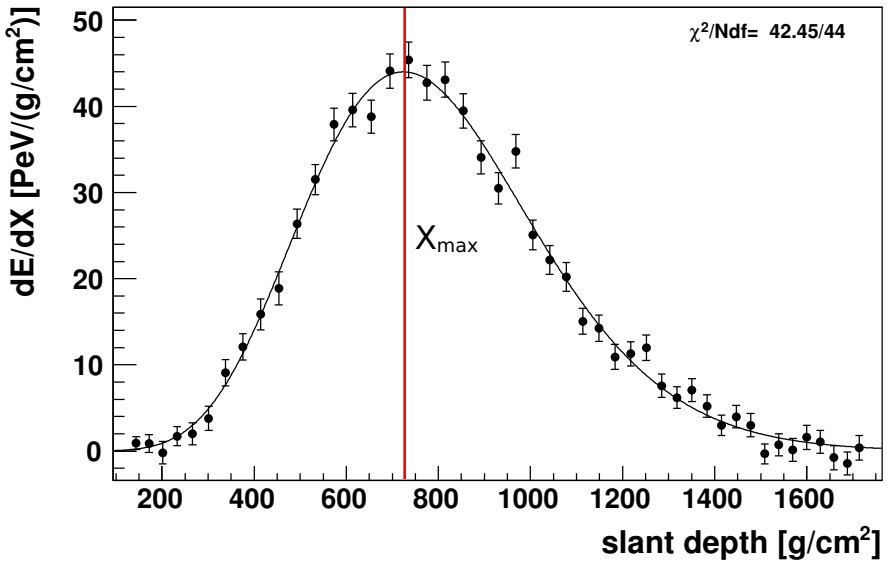

Figure 2.4: Longitudinal profile of a shower measured by the Pierre Auger Observatory. Shown is the energy deposit as a function of the slant depth which is proportional to the number of particles of the shower. The black line shows a Gaisser-Hillas fit of the profile, the red line marks $X_{\max}$. Adapted from [7].

Some attributes of this profile are described by the relatively simple Heitler model [8]. How a shower looks in the Heitler model is shown in figure 2.5. The model for the electromagnetic component assumes that the electrons and photons of the shower interact after passing a constant atmospherical depth X_0 and produce two new particles with half of the energy of the initial particle by bremsstrahlung and pair production processes. These two new particles then repeat the procedure unless their energy is lower than a critical energy E_c. The Heitler model reproduces the two important air shower properties which are the total number of particles at the shower maximum is proportional to the energy of the primary particle,

$$N(X_{max}) = \frac{E_0}{E_c} \tag{2.2}$$

and the depth of the shower maximum increases logarithmically with an increasing primary particle energy.

$$X_{\max} = \frac{X_0 \ln\left(E_0/E_c\right)}{\ln 2} \tag{2.3}$$

To describe the longitudinal shower profile more precisely a function proposed by Gaisser and Hillas is often used:[10]

$$N(X) = N_{\max}\left(\frac{X - X_0}{X_{\max} - X_0}\right)^{(X_{\max}-X)/\Lambda} \exp\left(\frac{X_{max} - X}{\Lambda}\right). \tag{2.4}$$

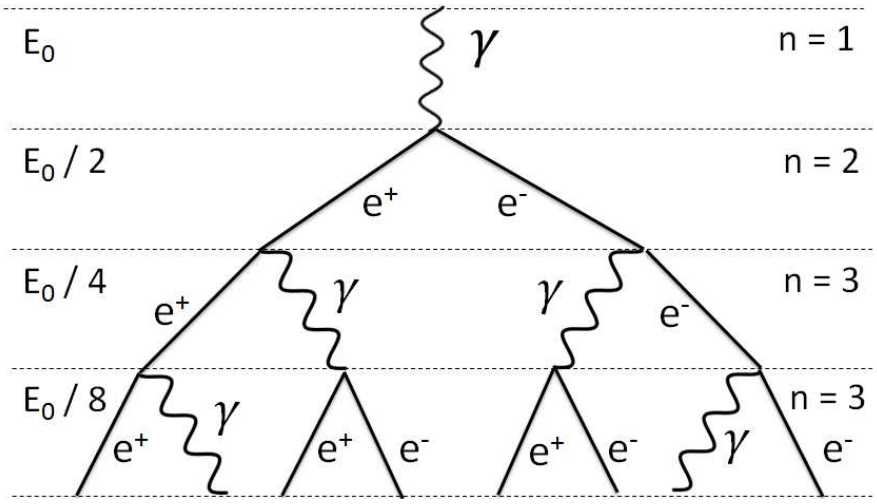

Figure 2.5: Sketch of the Heitler model. Electrons and photons of the shower interact after passing a constant atmospherical depth X_0 and produce two new particles with half of the energy of the initial particle. Taken from [9].

This Gaisser Hillas function describes the number of particles $N(X)$ as a function of traversed atmospheric depth X which is a parameter describing how much matter has been passed by the cosmic ray. In this formula X_0 and Λ depend on the primary particles mass and energy. $X_{\max}$ represents the atmosperic depth of the shower maximum, where the maximal number of particles is observed.

2.3 Fluorescence light detection technique

As figure 2.3 shows the most important component for the detection with fluorescence light detectors is the electromagnetic component. Particles with short lifetimes, such as the neutral pion, decay [6]. For the neutral pion the main decay channel produces two photons. These two photons with energies above 1022 keV decay to an electron and a positron, which both emit bremsstrahlung. This process is repeated so that a large number of lower energy particles is created. For lower energies referring to the Bethe formula these particles deposit more energy and therefore excite air molecules such as nitrogen. When the excited molecules return to a lower energy state they emit photons which we call the fluorescence light.

The fluorescence light detection technique measures the number of photons emitted by the shower as a function of position. It is commonly agreed that the number of the emitted photons is proportional to the deposited energy, with the fluorescence yield Y as constant of proportionality $N_{\text{photon}} = Y \cdot E$, so that the longitudinal energy deposit shower profile is measured implicitly [11].

To reconstruct the energy of the primary particle the deposited energy can be integrated. The small fraction of energy carried by neutrinos and other particles which do not emit fluorescence light can be corrected by multiplication

with a factor between 1.07 and 1.17. Since the fluorescence yield and its dependence on the atmospherical parameter is not measured exactly, the deposited energy is measured with an uncertainty of approximately 14% [12].

Figure 2.6 shows the wavelength distribution of an air shower measured by the AIRFLY experiment. It can be seen that most of the fluorescence light has wavelength between 300 and 400 nm. This fact can be used to reduce the background of measurements by using UV pass filters.

Using the time the fluorescence light arrives at and the direction it comes from the shower axis can be determined. This is described in a later section.

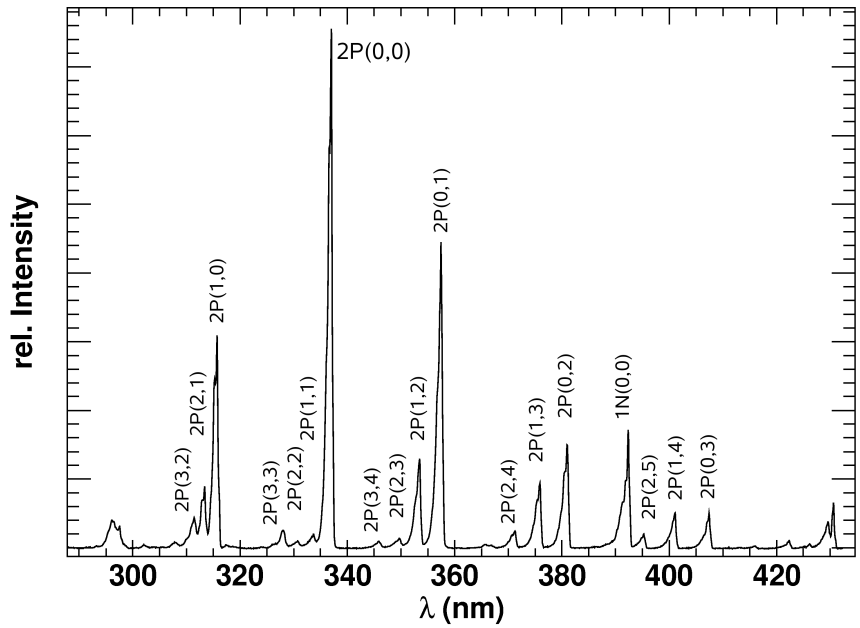

Figure 2.6: Fluorescence light spectrum of air as measured by the AIRFLY experiment with an electron beam of 3 MeV. The measurement was performed at 20°C and a pressure of 800 hPa. For each peak the initial state as quantum number as (ν', ν'') is given. Taken from [13].

3. The Pierre Auger Observatory

In the 1980's it was recognised that due to the small number of events at energies above 10^{19} eV areas of above 1000 km^2 would be needed to investigate UHECRs with sufficient statistics to discover new science (GZK-Cutoff). In 1991 and the following years, studies about the so-called Giant Air shower Project (GAP), later named Pierre Auger Observatory, in honour of Pierre Augers work on extensive air showers, were made [5]. In 2001 near Malargüe, Argentina the construction of the observatory began and was finished mid-2008. Figure 3.1 shows a sketch of the Pierre Auger Observatory. Dots show the positions of surface detector stations, while the blue lines segment the field of view of the 24 fluorescence telescopes located in four buildings at Los Leones, Los Morados, Loma Amarilla and Coihueco.

3.1 The surface detector

The surface detector consists of 1600 water Cherenkov detector stations in a triangular grid with a 1.5 km spacing covering an area of more than 3000 km^2 [6]. Figure 3.2 shows a scheme of a detector station. Each station consists of a 1.2 m deep water tank containing above 12 m^3 of pure water. On the top three photomultiplier tubes (PMTs) looking from the top of the tank to the bottom are placed. Particles passing the water tank with a velocity higher than the speed of light in water emit Cherenkov light which is detected by the PMTs.

The Pierre Auger Observatory, being located at an altitude of approximately 1400 m means that the detector is positioned beneath 880 g / cm^{-2} which is near the shower maximum for vertical showers in the investigated energy range [6]. If a shower hits three or more surface detectors, the shower geometry can be reconstructed using the time and position information recorded by the detector. In contrast to the fluorescence detector the surface detector measures high energy particles instead of light and therefore is not affected by ambient light so that measurements can be performed with an uptime of nearly 100%.

3.2 The fluorescence detector

The 24 fluorescence telescopes are housed in four buildings (at Los Leones, Los Morados, Loma Amarilla and Coihueco) [15]. Additional three fluorescence

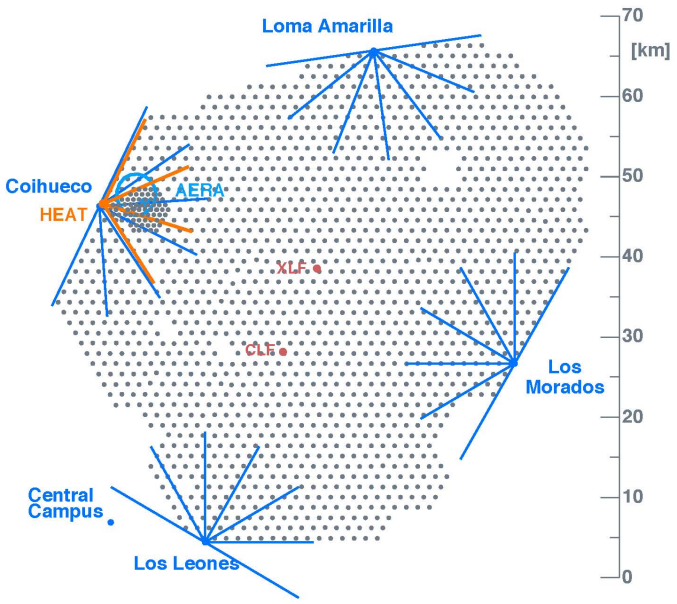

Figure 3.1: Map of the Pierre Auger Observatory in 2013. Dots show the positions of surface detector stations, while the blue lines segment the field of view of the 24 fluorescence telescopes which are located in four buildings on the perimeter of the surface array. Also shown are the infill array of the AMIGA experiment and the 3 HEAT fluorescence telescopes near the Coihueco station and the position of the Central and eXtreme Laser Facilities (CLF, XLF) indicated by red dots [14].

telescopes of the HEAT experiment are located at Coihueco to study cosmic rays with an energy down to 10^{17} eV [16]. Figure 3.3 shows the setup of one fluorescence telescope. Each telescope covers an azimuth of 30° and 28.1° elongation using 440 pixels arranged in a 22x20 hexagonal grid so that one housing has a field of view of 180° azimuth. Since the fluorescence telescopes need clear, moonless nights, they only can perform measurements with a duty cycle of approximately 13%. However the fluorescence telescopes are able to investigate the longitudinal shower profile and therefore add needed information to determine the primary particles mass composition.

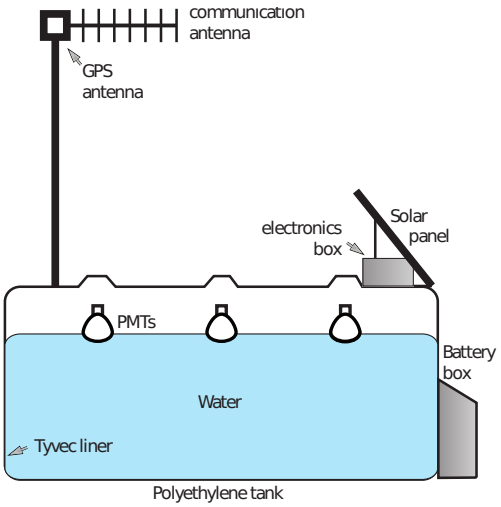

Figure 3.2: Scheme of a Pierre Auger Observatory Cherenkov detector taken from [5]

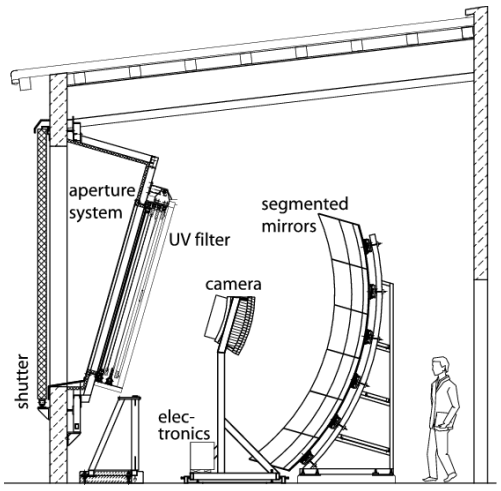

Figure 3.3: Scheme of a Pierre Auger Observatory fluorescence telescope. Taken from [15].

4. FAMOUS

Figure 4.1: Photo of FAMOUS adapted from [17].

FAMOUS (First Auger Multi-pixel-photon-counter-camera for the Observation of Ultra-high-energy-cosmic-ray air Showers) is a prototype fluorescence telescope for the detection of UHECRs based on silicon photomultipliers (SiPMs). The photomultiplier tubes (PMTs) commonly used in fluorescence telescopes offer photodetection efficiencies of approximately 35%. Currently, SiPMs already reach these efficiencies and prototypes promise detection efficiencies up to 60% [18]. Moreover, SiPMs offer the advantages of low supply voltage and potentially low costs. However alongside with this advantages come new challenges such as the high dark noise rate, a small sensitive area and a high

temperature dependency. A seven pixel prototype has already been built and first tests have been undertaken in Aachen, Germany.

4.1 Baseline design

To collect the faint fluorescence signal, an optical system of a Fresnel lens and Winston cones is used. The Fresnel lens with a diameter and a focal length of 502.1 mm and 10 grooves per mm is placed in the front of a aluminum tube [18]. The Fresnel lens focuses the fluorescence light on the Winston cones placed at the back of the housing with an efficiency of 70%. To increase the sensitive area, Winston cones collect the light passing through a disc with a diameter of 13.42 mm and concentrate, for incidence angles under 26.6°, 90% of the light on a disk with 6 mm diameter. This configuration leads to an effective field of view per pixel of 1.5° so that the full field view of the 64 pixel FAMOUS telescope is $\approx$ 12°. Behind the Winston cone an UG11 UV pass filter is placed. The light transmission of the UG11 UV-pass filter is shown in 4.2. Due to the high transmission efficiencies in the range of 270 to 370 nm wavelength most of the fluorescence light is transmitted while the majority of the light of ambiguent light sources such as stars and night sky itself is rejected. Shown in figure 2.6 the fluorescence light has large portions of its energy in the highly transmitted wavelength, so that the signal to noise ratio (SNR) can be increased effectively [19].

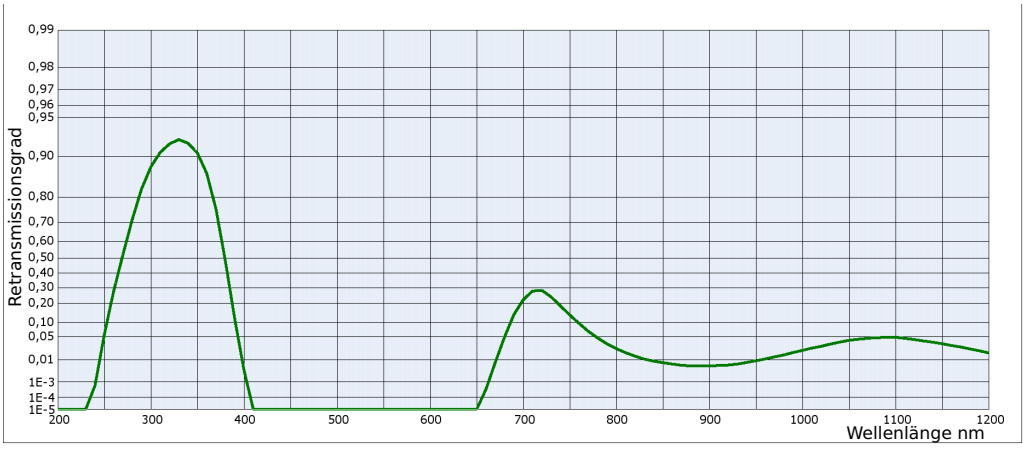

Figure 4.2: Light transmission of the UG11 filter for a thickness of 1 mm adapted from [19].

4.2 Silicon photomultipliers

Silicon photomultipliers (SiPMs) are relatively new developed single photon detectors. Their gain of 10^6 and photon detection efficiency are comparable to PMTs, but in comparison to conventional PMTs SiPMs are much smaller and need lower supply voltages of below 100 V.

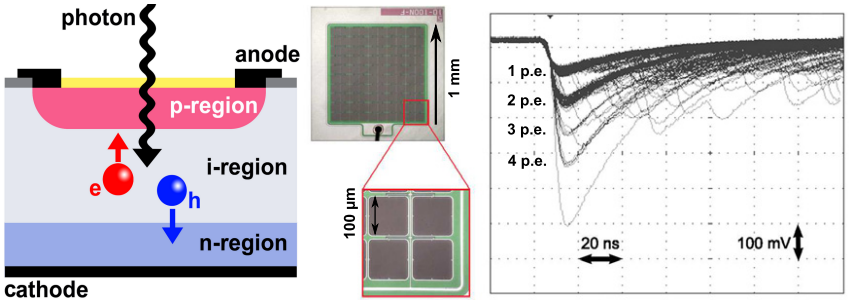

Figure 4.3: Left: scheme of the structure of a Geiger-mode avalanche photodiode. Center: photo of an SiPM with 1 mm^2 sensitive area and 0.1 mm cell pitch. Right: oscilloscope screenshot of amplified SiPM signals of noise. The signals can be allocated to the different numbers of cell breakdowns. (p.e.= photon equivalent). Adapted from [20] and [18].

SiPMs have sensitive areas of few square millimetres divided into typically over 100 individual Geiger-mode avalanche photodiodes per square millimetre all being connected parallel to a common load [18]. Despite each cell only being able to detect one photon at a time, this substructure allows the SiPM to generate a signal proportional to the number of impinging photons. Each cell mainly consists of an n- to p-doped semiconductor junction. In the area of contact, in a neutral state, a zone of depletion arises where holes and electrons recombine. To operate the cells in Geiger-mode, this area is enlarged by applying a reverse voltage V_{bias}. Usually, this voltage V_{bias} is adjusted slightly higher than the voltage V_{break} needed for the cell to work in Geiger-mode. The difference between these two voltages is refered to as over-voltage $V_{\text{ov}} = V_{\text{bias}} - V_{\text{break}}$. If a photon passes the depletion zone it can be absorbed and can create an electron-hole-pair. Both the electron and the hole are accelerated by the electric field and can cause further creation of electron-hole-pairs so that an avalanche is started. Since holes and electrons are accelerated in different directions this avalanche is self-sustaining. To stop the avalanche, a quenching resistor is connected in series to the cell. With the rise of the avalanche the current voltage drop over the quenching resistor increases so that the voltage drop over the cell decreases and the avalanche is stopped.

However an electron-hole-pair can also be created by thermal excitation so that an avalanche, which is indistinguishable from a non-thermal avalanche, is started [20]. Currently the thermal noise rate for SiPMs is in the orders of 100 kHz per mm^2, but the reduction of the noise rate is in progress. Additionally, correlated noise, namely cross talk and afterpulsing, exists. If an electron and a hole recombine and emit a photon this photon can trigger a neighbour cell. Afterpulsing is caused by charge carriers which were trapped at impurities of the silicon. If the charge carrier is released it can cause a new avalanche which is indistinguishable from a avalanche started by a photon. The probability for cross talk and afterpulsing depend on the over-voltage and are between 10% and 40%.

5. Data simulation

To simulate how a primary particle of the cosmic rays evokes a shower of secondary particles which emit fluorescence light that finally hits the FAMOUS's SiPMs three simulation frameworks are used.

5.1 Extensive air shower simulation with CONEX

For the simulation of the longitudinal shower profile CONEX is used. CONEX is program related to CORSIKA (COsmic Ray SImulation for KAscade) developed by the Karlsruhe Institute of Technology (KIT). To reduce the computation time CONEX simulates only the highest energy interactions with a Monte Carlo simulation, as CORSIKA, but solves corresponding cascade equations for the lower energy part of the shower [21]. CORSIKA offers the option to use several high energy interaction models. In this thesis the CONEX v2r3.1 version and the EPOS-LHC model are used. For azimuth angle from 0 to 330° in steps of 30°, zenith angles from 0 to 60° in steps of 10° and protons with energies from $\log_{10}\left(\frac{\mathrm{E}}{\mathrm{eV}}\right) = 16.5$ to $\log_{10}\left(\frac{\mathrm{E}}{\mathrm{eV}}\right) = 19.0$ in steps of 0.5, 10 showers for each configuration have been simulated. Additionally one shower with an energy of $\log_{10}\left(\frac{\mathrm{E}}{\mathrm{eV}}\right) = 10$ has been simulated and is used for the simulation of the night-sky background and the SiPM dark noise.

5.2 Fluorescence light simulation with Auger Offline

To simulate the fluorescence light emitted by the shower and its propagation through the atmosphere to the telescope the $\overline{\text{Off}}\underline{\text{line}}$ software package is used. For this purpose the $\overline{\text{Off}}\underline{\text{line}}$ software package generates a number of photons proportional to the energy deposit along the longitudinal binned shower profile provided by the CONEX simulation. The photon propagation through the atmosphere is computed for bundles of up to 512 photons, to increase the speed of the simulation, by Monte Carlo methods. Photons, which arrive at the telescope are saved in a ROOT file that later is read by a Geant4 simulation of FAMOUS.

The simulation of the fluorescence light propagation has been done for different distances R_p describing minimal distance between the shower axis and the telescope. Combinations of energy and R_p which the FAMOUS telescope can not

detect due to the low number of photons are not simulated to save computing time. This combinations have been identified in previous work [22].

5.3 FAMOUS detector simulation (Geant4)

For the simulation of the FAMOUS telescope Geant4, a toolkit for the simulation of the passage of particles through matter, developed at Cern is used [23]. The FAMOUS simulation reads the photons energy, position and momentum from the root file generated by Offline and adds photons to simulate the Aachen night sky background. Then the passage through the optical system consisting of Fresnel lens and Winston cones and the propagation through the UG11 UV pass filter is simulated. For the SiPM simulation the software package G4Sipm, developed by the RWTH III. Physikalisches Institut A, is used which incorporates a simulation the behaviour of SiPM's considering afterpulsing dark noise and cross talk and digitises the SiPM signal. The digitised SiPM signal is written in a ROOT file and is later read out and filled in a histogram with 200 bins with a width of 50 ns to be able to trigger on it.

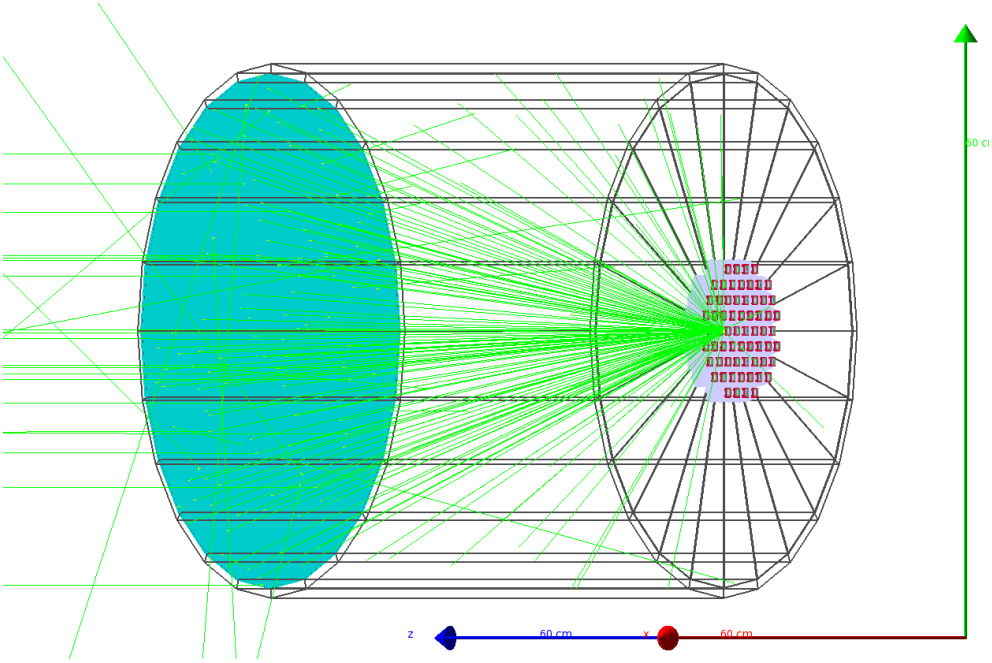

Figure 5.1: Geant4 simulation of FAMOUS with a testbeam of 100 photons

6. Event trigger

Since it is impossible to store all the data FAMOUS records a preselection of the data has to be done. For this purpose a trigger system is used. This system requires to record most of the interesting data when fluorescence light of showers arrive at the telescope, while recording as low background as possible.

6.1 Trigger layout

In this thesis a trigger layout based on three trigger levels is discussed. The first level trigger T1 triggers on single pixels which detect photons. The second level trigger T2 tries to identify patterns in the positioning of T1 triggered pixels and the third level trigger T3 uses the time information of the pixels to make a further selection.

6.1.1 Single pixel trigger T1

The single pixel trigger (T1) examines the voltage trace generated by one single SiPM as described above. In this simulation the trace contains the number of detected photons, multiplied by a weight between zero and one, in an interval of 10 μs, with a bin width of 50 ns. Generally, this information would be used to simulate the voltage drop over the SiPM as a function of the time but under the assumption that the recovery time of the SiPM is smaller than the bin width of 50 ns the trace can be used directly. This approach saves a lot of computation time. The weight equals one for most of the detected photons, but can be smaller if the SiPM cell did not recover completely from the previous breakdown. If the telescope looks perpediculary to the shower axis at cosmic rays with a minimal distance R_P between the telescope and the shower, all photons in the field of view of one pixel (1.5°) arrive with a maximal time difference of:

$$\Delta t \approx \sin 1.5\,^\circ \cdot \frac{R_p}{c}. \tag{6.1}$$

With c as the velocity of light.

Even for showers with an R_p of 8 km, which is the maximum R_p investigated in this thesis, Δt is smaller than 700 ns so that sharp peaks in the SiPM pixel trace can be observed. The T1 trigger tries to identify these peaks by looking at the bin values in relation to the mean value for the whole trace. To be less susceptible to randomly high bins, caused by cross talk, and since most signal

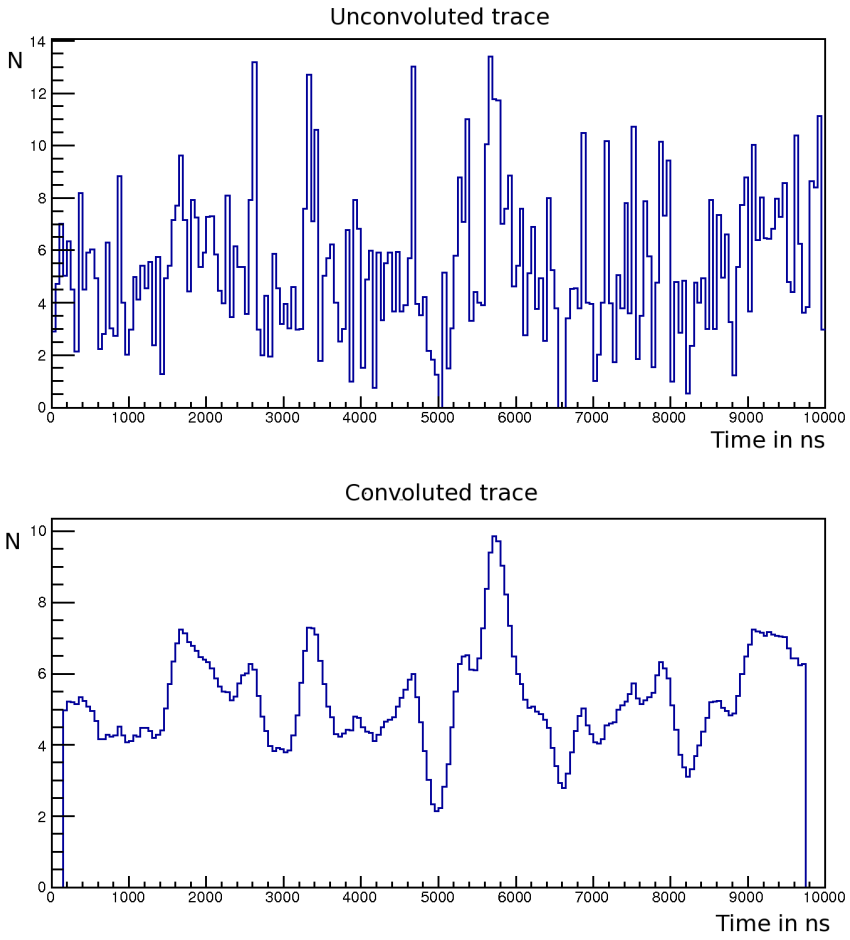

Figure 6.1: Top: unconvoluted trace. Botton: convoluted trace. Without convolution the bins at 2600, 3400, 4800 and 5700 ns are almost equally significant. With convolution the bin at 5700 ns is clearly distinguishable from the other bins.

peaks should be wider than the 50 ns bin width, a moving average is built by convolving with the triangular function with the width of 9 bins and an integral of 1. A trace before and after convolution is shown in figure 6.1. The convoluted trace is more sensitive to groups of high bins, which are expected for showers.

Due to SiPM noise and diffuse night sky the background follows a distribution remembering of a Poisson distribution. For this reason T1 triggers if the moving average at one bin i M_i exceeds the trigger threshold.

$$M_i > \mu + \lambda \cdot \sqrt{\mu} \tag{6.2}$$

The formula symbol μ describes the mean number of photons for the whole 10 μs interval per bin. The parameter λ, which roughly lies between 2.0 and 3.5,

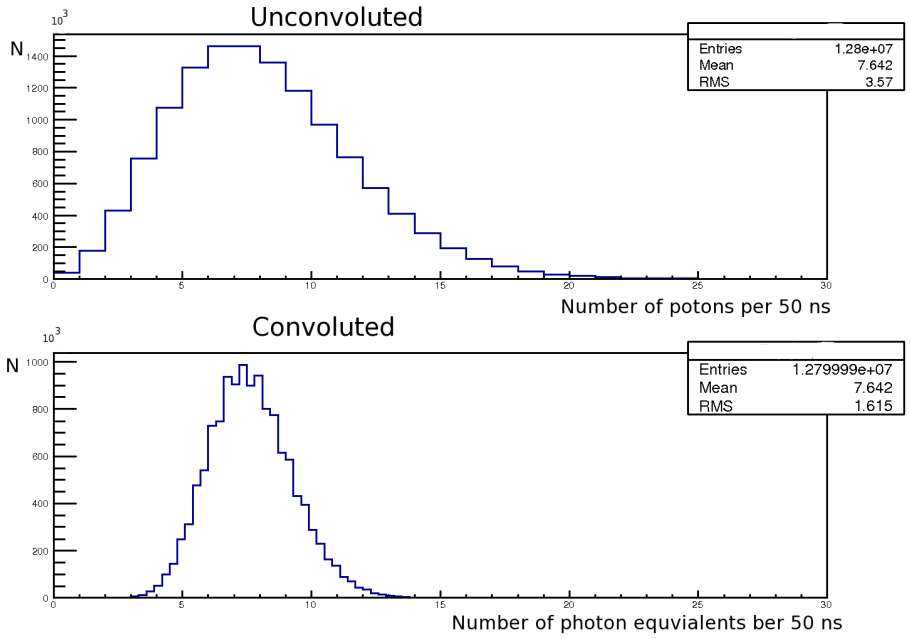

Figure 6.2: Distribution of photons per bin. Top: before convolution. Botton: after convolution. It can be seen that the convolution sharpens the distribution.

characterises the T1 trigger and will be determined later. This definition of the T1 trigger has the advantage to be insensitive on constant high background. If the light of one bright star shines in one pixel μ increases for this pixel so that the probability to trigger decreases slightly, whereas for a constant trigger threshold the probability to trigger would increase, which makes the telescope more stable against background. In the trigger simulations only the highest convoluted bin is kept even if T1 would trigger twice in a $10\,\mu$ time interval. This could be implemented in the experiment by waiting a short time for a higher signal before giving the information to the T2 trigger.

6.1.2 Position trigger T2

Since the Winston cones and therefore the field of view of the pixels is spherical and the packing density of the square grid is lower than the packing density of the hexagonal grid the FAMOUS pixels are arranged in a hexagonal grid.

6.1.2.1 Hexagonal grids

The points of a hexagonal grid can be described in different ways with different advantages and disadvantages [24]. In a hexagonal grid three primary axes, x, y and z can be identified with angles of 60° to each other. Cube coordinates use all three axes to determine a point in the hexagonal grid. In cube coordinates the sum of all coordinates is constant and set to zero here.
The relation $0 = x + y + z$ gives us the possibility to express one coordinate

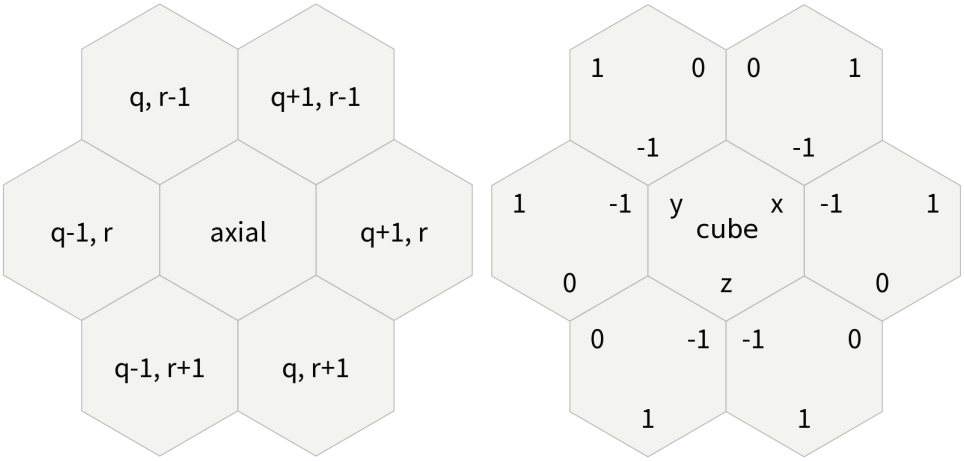

Figure 6.3: Left: axial coordinates, Right: cube coordinates. Adapted from [24].

by the other two. Axial coordinates are generated by using this redundance of the third coordinates so that the number of axes is reduced to two.

To calculate a distance between the two points (x_1, y_1, z_1) and (x_2, y_2, z_2) in a hexagonal grid it is easiest to use the cube coordinates.:

$$d = \frac{|x_1 - x_2| + |y_1 - y_2| + |z_1 - z_2|}{2}. \tag{6.3}$$

However axial coordinates have the advantage of the easier possibility to storing a hexagonal map in a two dimensional array with the indices of q and r, which is needed for the implementation of the T2 and T3 trigger.

6.1.2.2 T2 algorithm

The position trigger T2 seeks T1 triggered pixels which are connected to other T1 triggered pixels. Neighbouring pixels are considered to be connected. Figure 6.4 shows how a shower looks before the T2 trigger. For this shower the T2 trigger rejects the two pixels on the left side.

Especially for lower energy showers, whose light is focused between of two pixels and therefore might not be detected, if only pixels in contact are considered connected, the detection rate can be increased if pixels that are connected to the central pixel by the edge of two of the neighbours in contact of the central pixel are considered to be neighbours too. Figure 6.5 shows such a shower with two different values of λ. For the very small chosen value of λ in the left panel also the line of pixels to the left side triggers T1, since the small amount of light that is not focused perfectly between the pixel is enough to exceed the smaller λ T1 trigger threshold. For the higher λ T1 trigger threshold the left line does not trigger, but using the twelve possible connected pixels methode the shower is still detected.

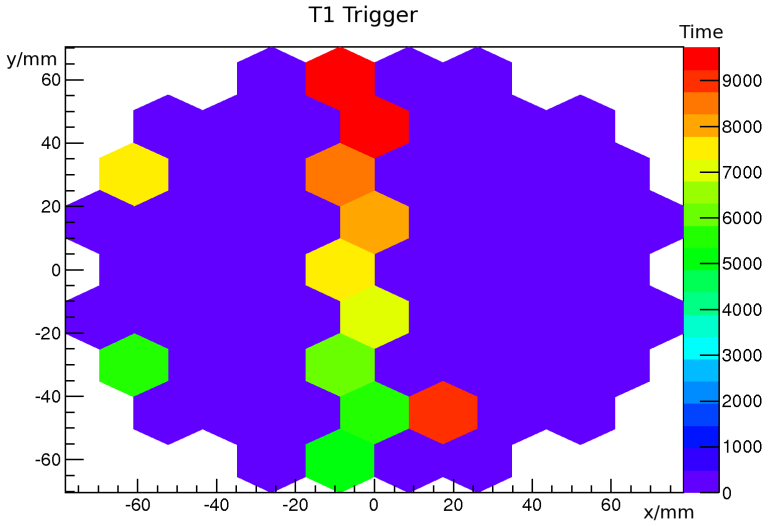

Figure 6.4: Shower with $\log_{10}(\frac{E}{\mathrm{eV}}) = 19$, $R_p = 8\,\mathrm{km}$, azimuth = 0°, zenith = 0° before T2 trigger. Pixels that do not possess two neighbours or one who has two neighbours are rejected. For this shower the T2 trigger rejects the two pixels on the left side but not the pixel to the right side of the shower, which is later rejected by the T3 trigger.

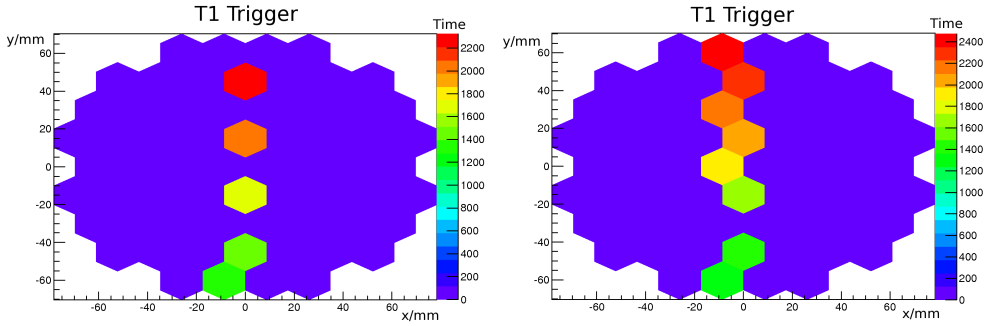

Figure 6.5: Shower with $\log_{10}(\frac{E}{\mathrm{eV}}) = 19$, $R_p = 8\,\mathrm{km}$, azimuth = 0°, zenith = 0° before T2 trigger. Left panel for $\lambda = 2.5$, right panel for $\lambda = 1.75$. A shower where the twelve neighbour pixel trigger does well since some of the light is lost in the space between the cones.

However both, decreasing the T1 threshold λ or increasing the number of possible connected pixels, increases the background rate, and therefore the best configuration needs to be examined.

The T2 trigger gets a list of x- and y- coordinates of the pixels which passed the T1 trigger in carthesian coordinates and transforms them to points in a two dimensional array representing the hexagonal grid in axial coordinates. In a loop over the two dimensional array the number of triggered connected

pixels is determined by testing all, dependent on the neighbour model, six or twelve neighbours. If a pixel has more than one triggered connected pixel all connected and T1 triggered pixels are marked as T2 triggered and written in another two dimensional array, which transformed back into x- and y-positions later. This implementation of T2 ensures that also pixels at the end of one trace with one T1 triggered connected pixel, who has two or more T1 triggered connected pixels, are triggered.

6.1.3 Time trigger T3

The T3 trigger is a very simple addition to the T2 trigger which almost lets pass all signals, but supresses the background by the order of one magnitude. In Figure 6.4 is a shower after the T1 trigger shown. After the two pixels on the left side are rejected by the T2 trigger the T3 trigger rejects the pixel on the right side.

The T3 trigger basically uses the same algorithm as the T2 trigger with the addition that only pixels with a difference in time which is less than a time τ, are considered to be neighbours. The probability for the T3 trigger to reject a background triggered pixel that passed the T2 trigger and is connected to one other T2 triggered pixel can be estimated to $1 - p = \frac{2 \cdot \tau}{10\,000}$. If the pixel is connected to two other pixels, which are T3 connected, the rejection probability is larger than $1 - p = \frac{3 \cdot \tau}{10\,000}$.

6.2 Trigger optimisation

The trigger for FAMOUS should be optimised ins such a way that as much cosmic rays as possible can be detected even for lower energies while keeping the background trigger rate as low as possible. Since the flux of cosmic rays with energies higher than $10^{18}\,\mathrm{eV}$ is in the order of $1\,\mathrm{km}^{-2}\mathrm{day}^{-1}$ but the trigger operates on timeframes of $10\,\mu\mathrm{s}$ triggering on one of roughly 10 billion background timeframes of $10\,\mu\mathrm{s}$ would equal a signal to noise rate of one.

6.2.1 Background simulation using the single pixel trigger rate

To simulate the background, the same framework which has been used to simulate cosmic rays, is used to simulate a shower with an energy of $10^{10}\,\mathrm{eV}$ in a distance of 4 km so that almost no photons arrive at the telescope. Since the simulation of $10\,\mu\mathrm{s}$ wide traces, even for backround only, takes more than 20 s computation time the time needed to simulate one day of background with a typical single core processor would exagerate 5000 years. To be able to simulate larger timeframes, 1000 times $10\,\mu\mathrm{s}$ for 64 pixels have been simulated. For the so generated $6.4 \cdot 10^4$ $10\,\mu\mathrm{s}$ intervals an average probability for a pixel to trigger T1 in dependence of λ has been determined. In a second step a large amount of pixels is generated and triggered with the given probability. For triggered pixels also a time between 0 and $10\,\mu\mathrm{s}$ is generated. If in a bundle

of 64 pixels representing 10 μs of FAMOUS looking at background more than 2 pixels are triggered, the list of pixels is passed to the T2 and T3 trigger to determine if this 10 μs background timeframe passes all trigger levels. This method decreases the computation time drastically but lacks of statistic for values of λ larger than 3.25 since for this value less than 10 of the simulated $6.4 \cdot 10^4$ pixels trigger in T1.

6.2.2 Single pixel trigger T1

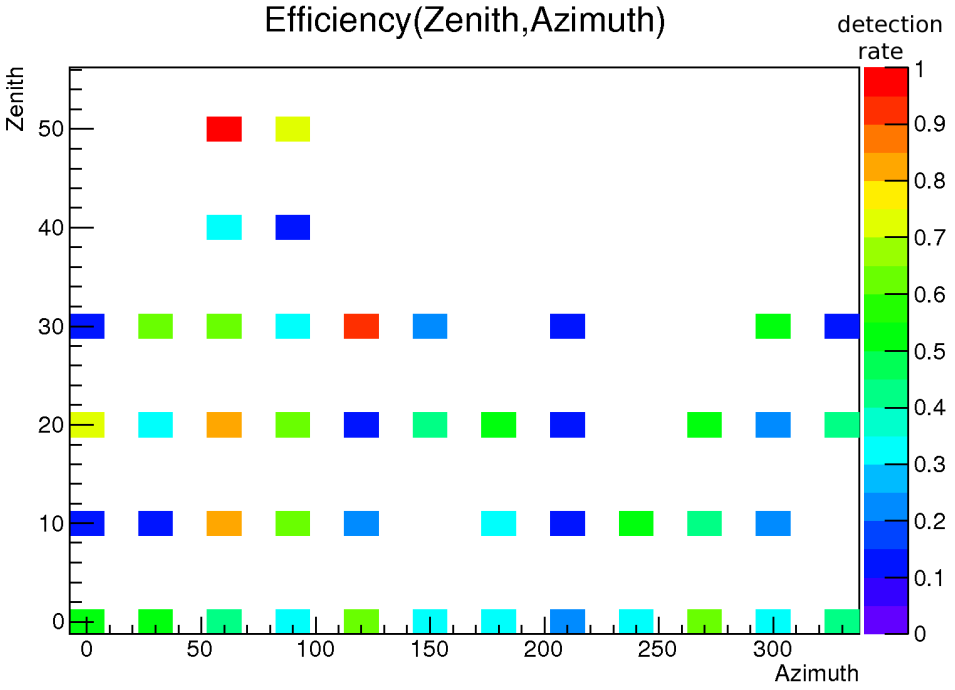

Figure 6.6: Efficiency of the full 3 level trigger in dependence of zenith and azimuth for showers with an energy $\log_{10}(\frac{E}{\mathrm{eV}}) = 17.5$ in a distance R_p of 1 km. The trigger parametrs are $\lambda = 3.0$, $\tau = 750$ ns, 6-neighbours

To optimise the parameter λ first the shower detection efficiency and the flux of detactable showers in dependence of the parameter λ are investigated at. After this, the dependency of the background on λ is determined.

6.2.2.1 Efficiency and flux of detectable showers

Figure 6.6 shows the detection rate of showers with energies of $\log_{10}(\frac{E}{\mathrm{eV}}) = 17.5$ and an R_p of 1 km for a parameter $\lambda = 3.0$. Showers with an zenith angle of 60° could not be detected.

In figure 6.7 the mean value, calculated from figure 6.6 for all investigated configurations of E and R_p, is shown. It can be seen that showers with an energy of $\log_{10}(\frac{E}{\mathrm{eV}}) = 16.5$ or 17 can not be detected with this trigger configuration.

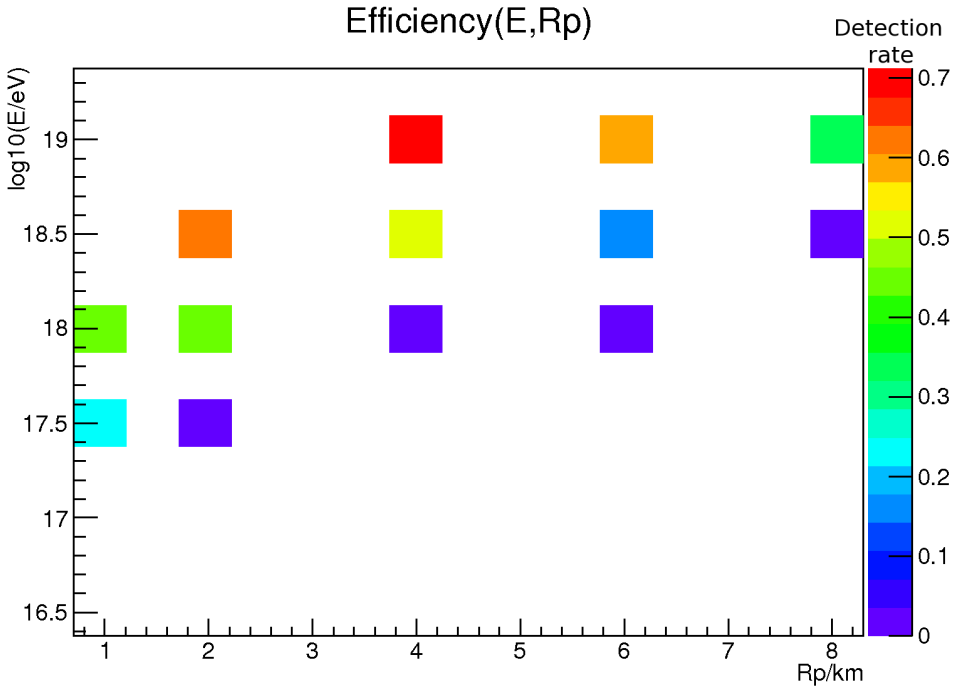

Figure 6.7: Efficiency for the full 3 level trigger with the parameters $\lambda = 3.0$, $\tau = 750\,\text{ns}$, 6-neighbours

This plot visualises the limit of detectable showers. The detection efficiency caps at 0.7 since showers with an zenith angle of 60° can not be detected.

Using the energy spectrum for cosmic rays the flux of showers detected can be estimated. For this purpose the field of view of FAMOUS of 12°, the distances R_p of the bin and the bin with the next smaller R_p are taken to calculate an area that showers can be detected in for each bin of Figure 6.7. In a second step the flux for one energy and the detection efficiencies for this configuration are taken to examine the flux for this configuration. To obtain the total flux of detected showers the results are added up. Figure 6.8 shows the flux of detected showers for different values of the parameter λ. Since the detection efficiency of the minimal shower energy and the maximum value of R_p is taken to calculate the flux of detected showers for one bin, the total calculated flux gives the lower limit.

6.2.2.2 Background flux

As described in section 6.2.1 the probability for a single pixel to trigger in dependency on the T1 parameter λ is determined, and a set of up to 10^{10} of $10\,\mu\text{s}$ intervals is created. Subsequently the number of timeframes of $10\,\mu\text{s}$, which would cause all three trigger levels to trigger, is determined. Finally it is calculated how often all three trigger levels would trigger per day. Table 6.1 shows the result for the T2 trigger with 6 possible neighbours and a maximal

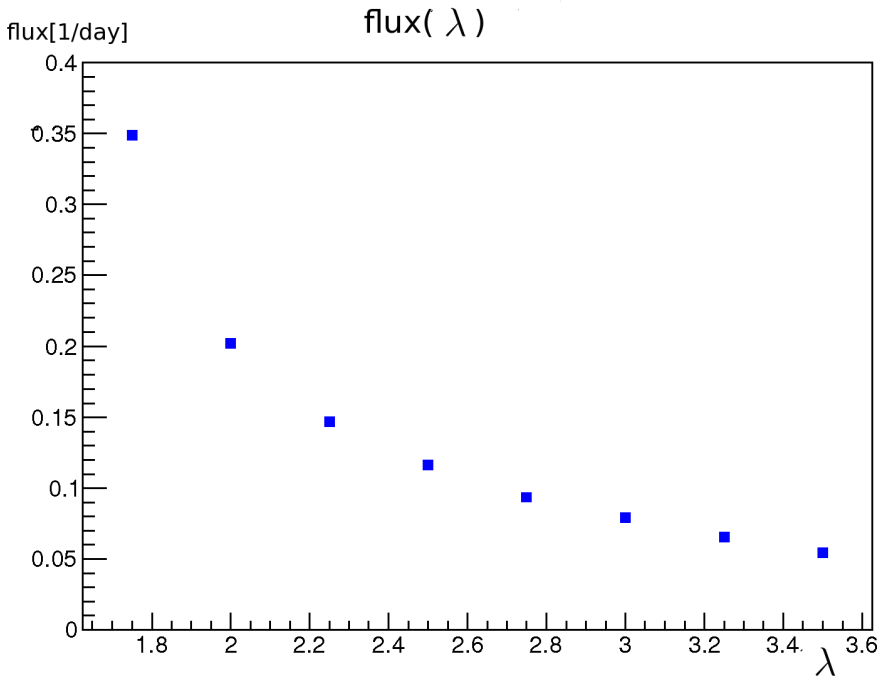

Figure 6.8: Flux of detected showers as a fuction of λ for constant $\tau = 750\,\text{ns}$ and the 6-neighbours methode

time difference of $\tau = 750\,\text{ns}$. For values of $\lambda \geq 3.25$ zero of the 10^{10} $10\,\mu\text{s}$ intervals have passed the T3 trigger so that the rate can be estimated to be smaller than $\frac{1}{\text{day}}$. The column background trigger T4 per day in $\frac{1}{\text{day}}$ shows the value of the background trigger rate if a fourth trigger criterion is used, which will be described later.

λ	probability for T1 trigger	Background trigger rate T3 in $1\,\text{day}^{-1}$	Background trigger rate T4 in $1\,\text{day}^{-1}$
1.75	0.20	$3.8\ 10^8$	$4.5\ 10^7$
2.0	0.080	$2.5\ 10^7$	$1.0\ 10^6$
2.25	0.028	$1.1\ 10^6$	$1.5\ 10^5$
2.5	0.0090	$4.3\ 10^4$	$4.3\ 10^2$
2.75	0.0026	$1.0\ 10^3$	< 10
3.0	0.00066	15	< 1.6
3.25	0.00013	< 0.86	< 0.86
3.5	0.000016	< 0.86	< 0.86

Table 6.1: Background trigger rates for the T3 and T4 trigger with the 6-neighbour configuration of T2.

6.2.2.3 Conclusion T1 optimisation

Due to the high background for low values of λ choosing values for $\lambda < 2.75$ makes little sense, since the noise to signal ratio in T3 would exceed 1000. Since the computation time to examine background trigger rates lower than one per day exceeds the extent of this work, no exact best value for λ can be given, but looking at the behaviour of the background trigger rate it can be said that for values of $\lambda \geq 3.5$ the background rate decreases to the order of $\frac{0.01}{\text{day}}$. For these values of λ the flux of detected showers is $0.05\,\text{day}^{-1}$ so that more than half of T3 triggered showers would be signal.

6.2.3 Position trigger T2

λ	probability for T1 trigger	Background trigger rate T3 in $1\,\text{day}^{-1}$	Background trigger rate T4 in $1\,\text{day}^{-1}$
1.75	0.20	$1.6\ 10^9$	$4.4\ 10^8$
2.0	0.080	$1.3\ 10^8$	$1.2\ 10^7$
2.25	0.028	$6.4\ 10^6$	$2.0\ 10^5$
2.5	0.0090	$2.1\ 10^5$	$2.5\ 10^4$
2.75	0.0026	$6.2\ 10^4$	62
3.0	0.00066	$1.4\ 10^2$	< 15
3.25	0.00013	< 0.86	< 0.86
3.5	0.000016	< 0.86	< 0.86

Table 6.2: Background trigger rates for the T3 and T4 trigger with the 12-neighbour configuration of T2.

Comparing table 6.2 to table 6.1 it can be seen that the addition of the 6 possible neighbours increases the bacground rate by a factor of between 5 and 10. However increasing λ by 0.25 leads to a decreasing of the backround by a factor of about 50. Since the detection efficiency decreases only slightly for an 0.25 increased λ using the twelve pixel T2 trigger should be the preferred option.

Figure 6.9 and 6.10 show the detection efficiencies of showers with the same trigger setup as 6.6 and 6.7, but for the twelve possible connected pixel methode. In the comparison it can be seen that especially for showers with low energy in a close distance the detection rate increases drastically. Since the energy spectrum falls with the power of $\gamma = -3.1$ in the estimated energy segment, this low energy showers constitute the majority of the measured showers, so that the flux of detected showers increaes significantly.

6.2.4 Time trigger T3

Formula 6.1 gives an approximation for the maximal time difference between the light which is focused on one pixel if the pixel of the telescope looks or-

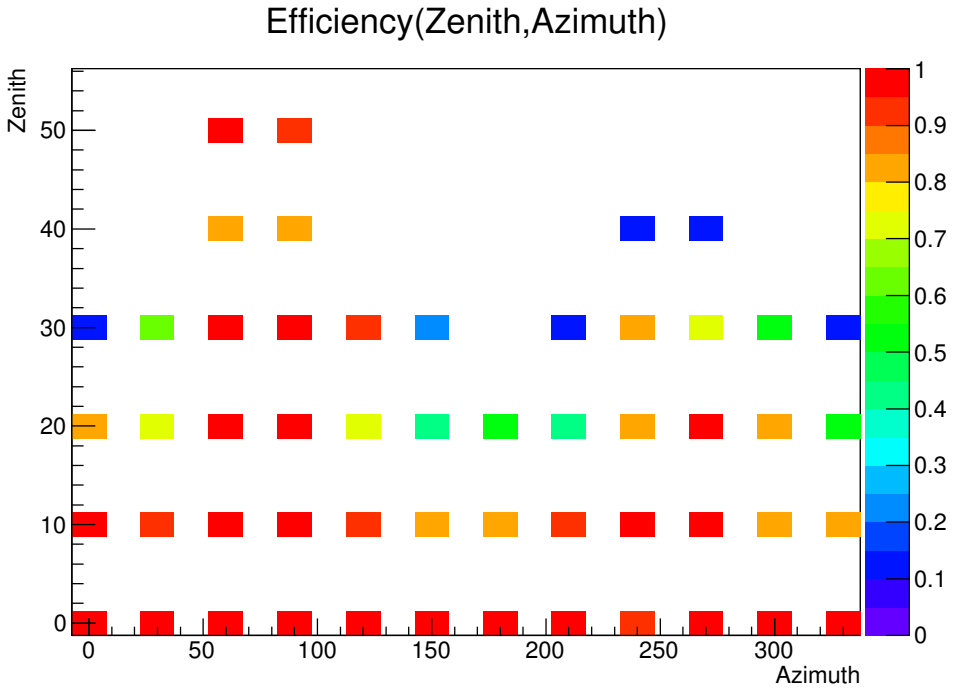

Figure 6.9: Efficiency of the full 3 level trigger in dependence of zenith and azimuth for showers with an energy $\log_{10}(\frac{E}{\mathrm{eV}}) = 17.5$ in a distance R_p of 1 km. The trigger parameters are $\lambda = 3.0$, $\tau = 750$ ns, 12-neighbours

thogonally to the shower axis at cosmic rays. For arbitrary pixels the relation is more complex, but a maximum for all pixels can be given to

$$\Delta t \leq \frac{R_p}{c} \cdot \frac{\sin(\Delta\chi)}{\sin^2(\pi - \chi_0)} \cdot (1 + \cos(\pi - \chi_0)) \tag{6.4}$$

Equality is reached for the pixels that look at the light emitted from the shower at ground level.In this formula the quantities refer to figure 7.1. The angle $\Delta\chi$ describes the difference of two angles χ_i and is 1.5° since this is the difference between two pixels. The angle χ_{R_p} names the value of χ_i for $t_i = t_0$. The formula shows that the parameter τ needs to be selected in dependence of the showers which shall be detected. For showers at a maximal distance of 2 km with a maximal zenith angle of 30° τ can be set to 400 ns without loosing detection efficiency even for the light with the highest difference between two pixels. In contrast to this for showers with R_p of 8000 km and a zenith angle of 60°, τ would need to be set to 5000 ns to be able to T3 trigger the fluorescence light which is emitted from the shower at ground level. If light emitted with a maximal difference $\chi_i - \chi_{R_p} = 6°$ for $R_p = 8$ km shall be detected τ needs to be be set to 780 ns. In this thesis τ is set to 750 ns for all analyses, since almost all showers investigated can be detected over the full 12° field of view of FAMOUS with this configuration.

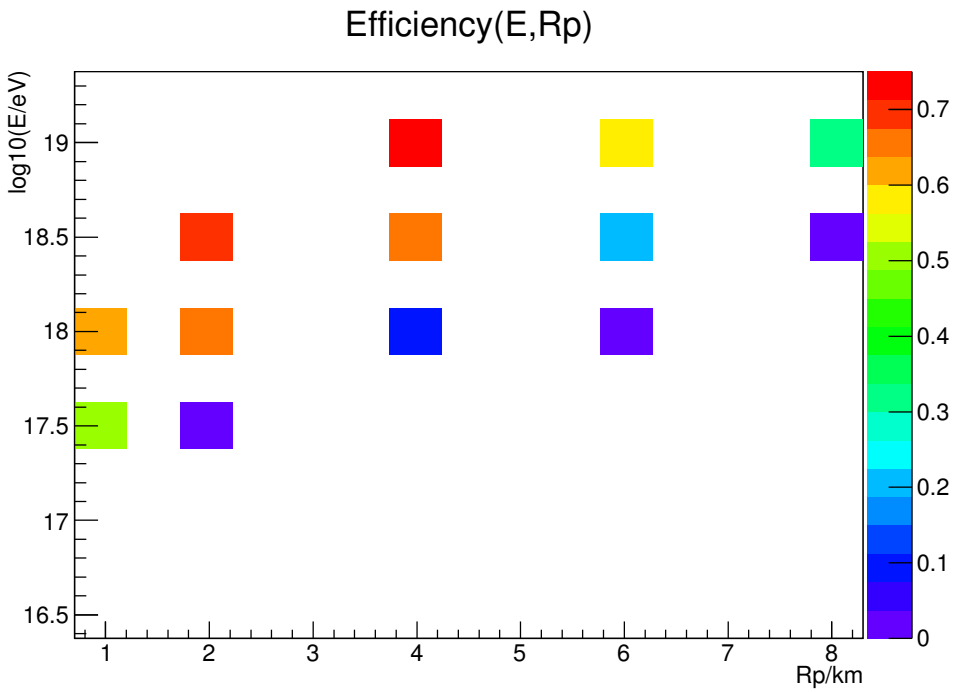

Figure 6.10: Efficiency for the full 3 level trigger with the parameters $\lambda = 3.0$, $\tau = 750\,\text{ns}$, 12-neighbours

6.2.5 Addition of a level 4 trigger T4

Figure 6.11 shows the number of pixels which pass the T3 trigger for signal and noise. It can be seen that more than 90% noise event consists of events which triggered three pixels, whereas for signal events the ratio is smaller than 20%. For higher values of λ this effect increases since the toal number of T1 triggered pixels decreases faster for noise than for data. As the tables 6.1 and 6.2 show for $\lambda = 2.75$ the rate of 3 pixel events in noise increased to approximately 99%, while the rate of 3 pixel events in signal remains almost unchanged as figure 6.11 shows. Due to this observations a level 4 Trigger T4 has been invented which rejects events with less than 4 T3 triggered pixels. The trigger criterion could also be tightened so that only events with more than 4 T3 triggered pixels are accepted.

6.3 Trigger simulation results

Figure 6.12 shows the detection efficiency in dependence of the shower parametrs. It can be seen that, due to the 12-neighbour T2 trigger, the detection rate of showers with lower energy at smaller distances R_p increased in comparison to other trigger setups despite the higher value of $\lambda = 3.5$. Since, as written above, the low energy showers constitute the majority of the flux the chosen trigger parameters lead to a flux of detectable showers of $9.8{\cdot}10^{-2}\,1\,\text{km}^{-2}\text{day}^{-1}$,

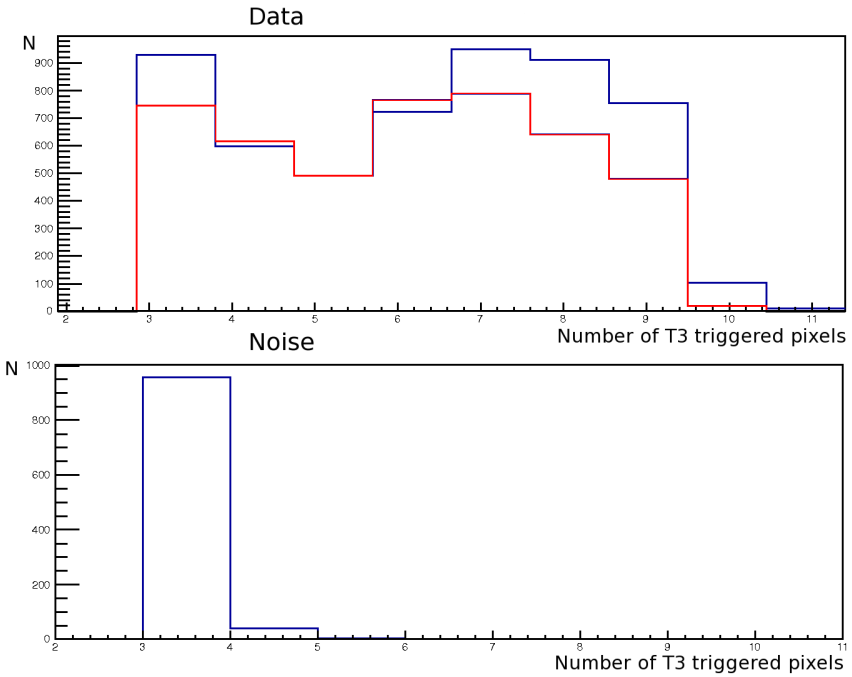

Figure 6.11: Number of pixels T3 triggered. Top: signal for $\lambda = 2.75$ in red and for $\lambda = 2.0$ in blue. Botton: noise for $\lambda = 2$

while the flux of background can be estimated to be in the order of $1 \cdot 10^{-3}$ $1\,\mathrm{km}^{-2}\mathrm{day}^{-1}$

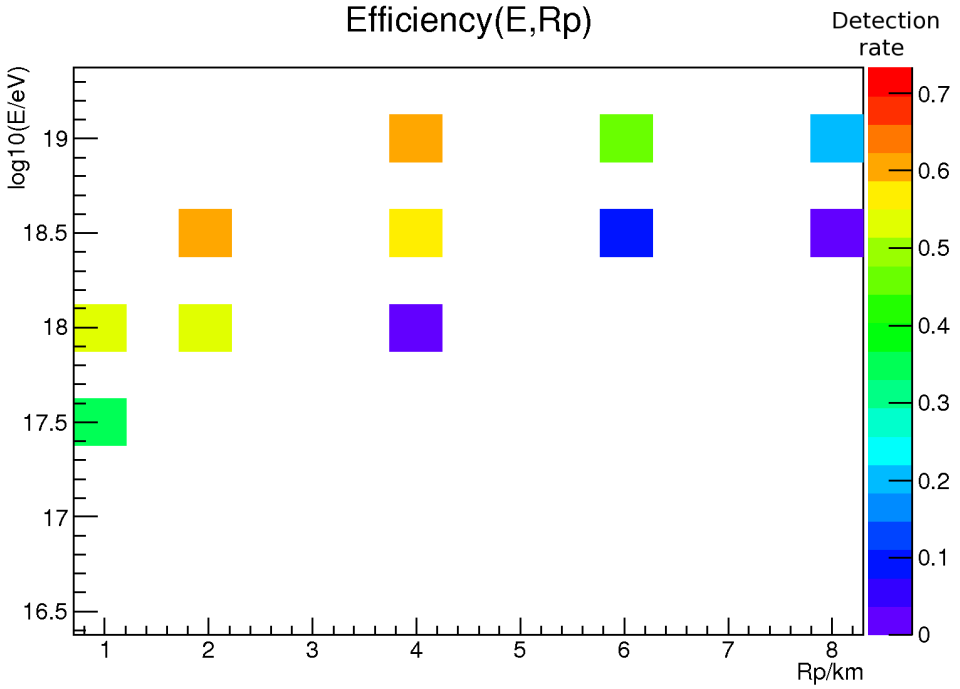

Figure 6.12: Efficiency for the final trigger with the parameters $\lambda = 3.5$, $\tau = 750\,\text{ns}$, 12-neighbours and the T4 trigger

7. Shower geometry reconstruction

7.1 Shower geometry

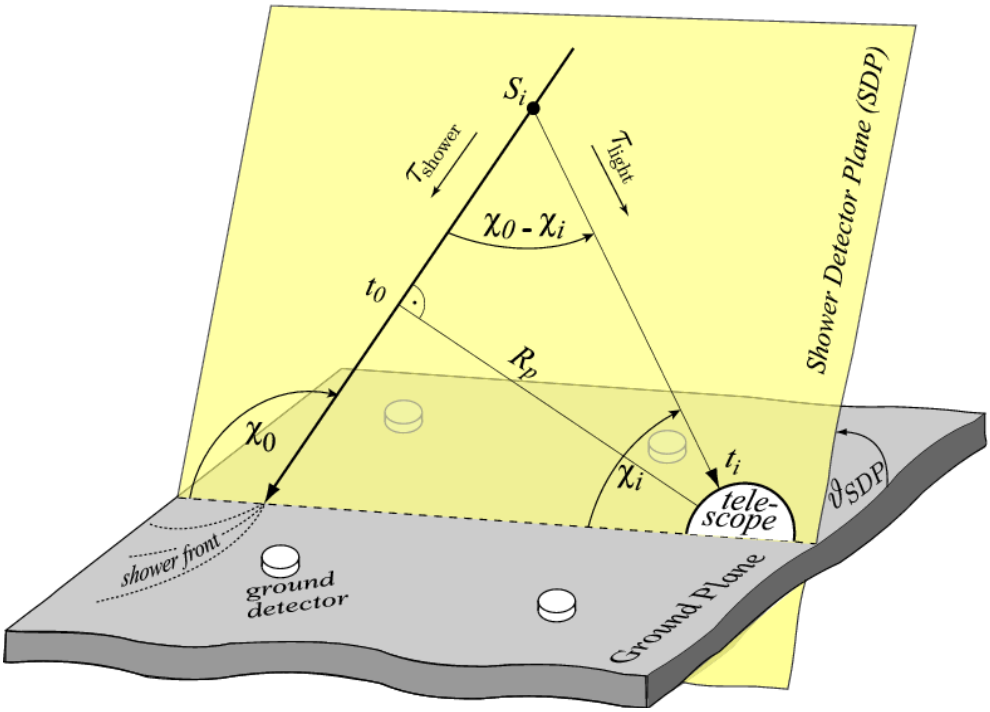

Figure 7.1: Sketch of the shower geometry and quantities used. Taken from [25].

Commonly, the geometry of showers, seen as a half-line in three dimensional space, is described by the use of the three parameters Θ_{SDP}, R_p and χ_0. The angle Θ_{SDP} is defined as the angle between the ground plane an the shower detector plane (SDP) and will later be the first parameter to be examided. The angle χ_0 is defined as the angle between the shower axis and the ground plane which lies in the SDP and R_p is defined as the minimal distance between the shower axis and the telescope. The points on the shower axis are described by the angle χ_i between the ground plane and the connecting line between the telescope and the point on the shower axis. Typically it is assumed that the

cosmic ray propagates with the same speed as the fluorescence light which is emitted instantaneously, so that the time the fluorescence light emitted from a certain point on the shower axis described by χ_i arrives at the telescope at the time t_i with the relation [25]:

$$t_i = t_0 + \frac{R_p}{c} \cdot \tan \frac{\chi_0 - \chi_i}{2} \tag{7.1}$$

7.2 Shower geometry reconstruction

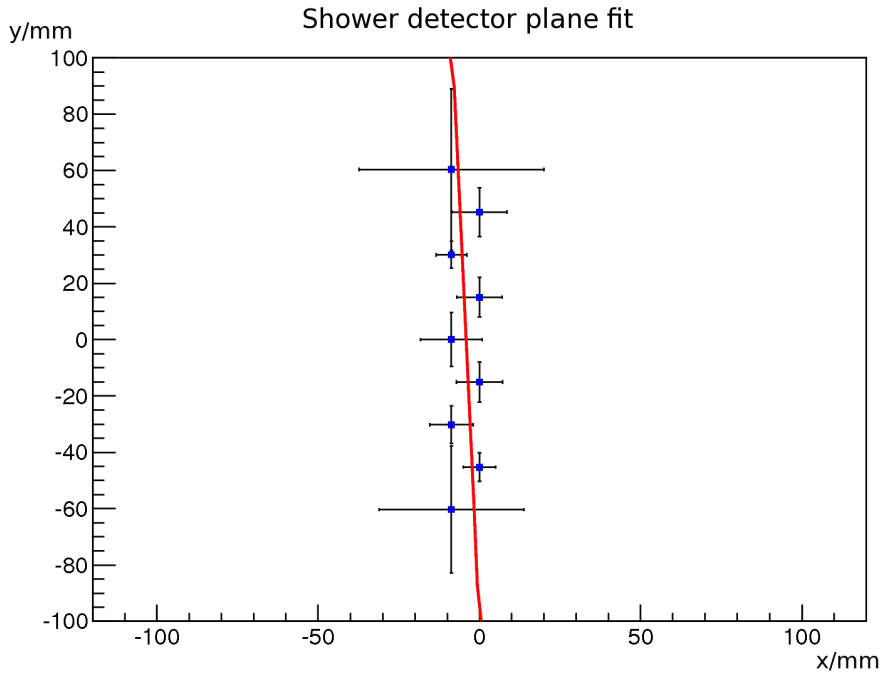

Figure 7.2: Fit of Θ_{SDP}. The error bars do not refer to errors of the x- and y- position but are a visualisation of the weight the pixels get for the fit. Smaller error bars mean that the pixel triggered more distinct in T1 trigger and therefore will be given more weight. Shower Parameter: $\log_{10}(\frac{E}{\mathrm{eV}}) = 19$, $R_p = 8\,\mathrm{km}$

To reconstruct the shower geometry, first the angle Θ_{SDP} is determined. As figure 7.2 shows, this is done by fitting a line to the pixel positions. It is important to note that the error bars plotted in 7.2 do not refer to errors but give a visualisation of the weight used for the position of each pixel. Pixels with smaller error bars have triggered more distinct in the T1 trigger and therefore are given more weight in the fit. The fit is performed as a 2-dimensional vectorial fit, since especially for Θ_{SDP} of 90° the slope diverges which could cause problems for a conventional straight line fit.

After the reconstruction of the shower detector plane the geometry of the shower within the plane, given by R_p and χ_0 can be determined. This is done by examining the dependency of the arrival time of the fluorescence light t_i at the pixels and the angle χ_i in the SDP the pixel looks at. To find the angle χ_i the positions of the pixels are projected to the fitted SDP. The best fitting geometry for equation 7.1 then can be determined. A fit of the parameters is shown in figure 7.3 for the shower Θ_{SDP} has been examined for.

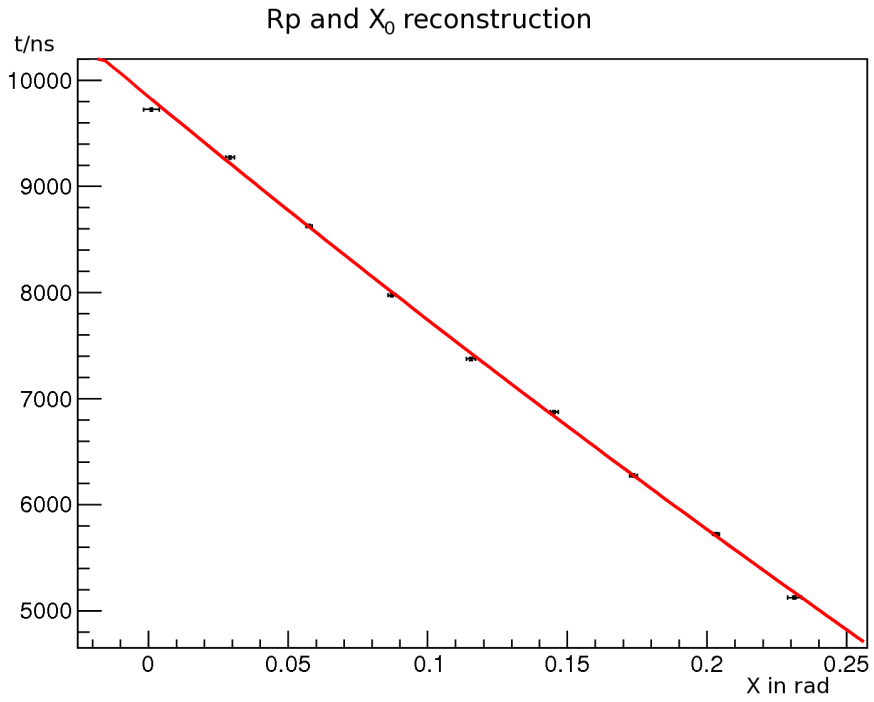

Figure 7.3: Fit of the parameter χ_0 and R_p. Shower Parameter: $\log_{10}(\frac{E}{\mathrm{eV}}) = 19$, $R_p = 8\,\mathrm{km}$

However as shown in figure 7.4 R_p and χ_0 are correlated, so that if R_p is decreased while χ_0 is increased the right amount, the time information the pixels would get is almost unchanged. In addition FAMOUS has a relatively small field of view, so that only a small part of the shower is observed, which increases the difficulties in the reconstruction further. For this reasons the rate of showers, whose parameters can be reconstructed successfully is very small. Using the time information at ground level of a SD-detector could help to increase the accuracy of the shower geometry reconstruction.

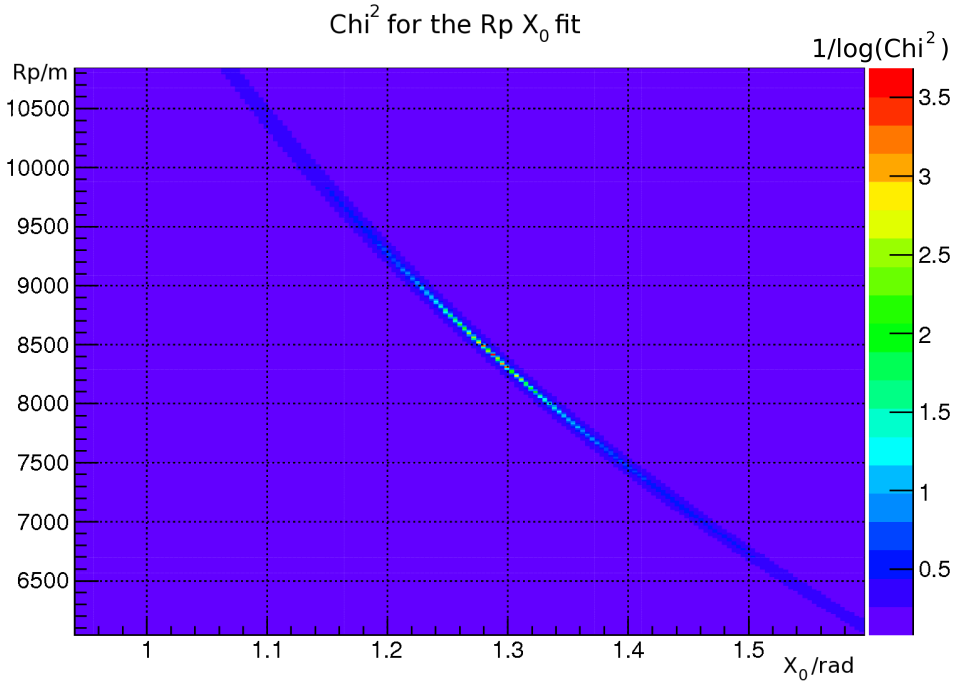

Figure 7.4: χ^2 for the shower geometry fit. The correlation between R_p and χ_0 can be seen. Shower Parameter: $\log_{10}(\frac{E}{\mathrm{eV}}) = 19$, $R_p = 8\,\mathrm{km}$. A minimum in χ_0 can be found for $R_p = 8\,\mathrm{km}$, but due to the correlation, mentioned above, many more minima can be found.

8. Summary and Outlook

Ultra high energies cosmic rays (UHECRs) entering the atmosphere of the Earth interact with the air particles causing so-called extensive air showers of secondary accelerated particles. To demonstrate tje feasibility of SiPMs for the detection of UHECRs, the project FAMOUS has been initiated. In a first step the night sky background and the brightness of several stars has been measured with a single pixel[26]. This year further measurements have been performed with a 7-pixel version of FAMOUS and the passages of stars through the pixels have been observed. The construction of a 64-pixel version of FAMOUS, which will be finished next year offers the possibility to detect traces of fluorescence light of cosmic rays. For this detection a trigger, which distinguishes the rare UHECRs from the bright background of the night sky is needed. In this thesis a trigger for cosmic rays with different energies, angles and distances to the telescope has been developed, based on simulated showers. For the generation of the background, the high computation time was discussed and a possible way to speed up the computation has ben found. A trigger setup consisting of 4 levels was proposed. The first trigger level triggers for single pixels if many photons arrive at the pixel in a short time span. Triggered pixels are then given to the second level trigger which seeks connected pixels indicating a trace of a cosmic ray. The third level trigger uses the time information to distinguish between randomly triggered background pixels and neighboured pixels with a small time difference. Finally the fouth level trigger considers the total amount of triggered pixels. This trigger setup has been optimised so that purities of 90% for a considerable high trigger rates, for the small field of view of FAMOUS, of $0.1\,\mathrm{km}^{-2}\mathrm{day}^{-1}$ can be reached. Furthermore the reconstruction of the shower geometry was performed and challenges and possible ways to improve the reconstruction were found. The next steps of the FAMOUS project will be further measurements with the 7-pixel FAMOUS version and hardware improvements and the construction of the 64-pixel FAMOUS version.

Bibliography

[1] Nobelprize.org. Henri Becquerel - Facts. Web., Sep 2014.

[2] Nobelprize.org. Nobel Prize in Physics 1936 - Presentation Speech.

[3] K.A. Olive et al. (Particle Data Group). Review of particle physics. *Chin. Phys. C*, 38:090001, 2014.

[4] The Pierre Auger Project Design Report. 1996.

[5] Karl-Heinz Kampert and Alan A Watson. Extensive Air Showers and Ultra High-Energy Cosmic Rays: A Historical Review. *arXiv physics.hist-ph*, Jul 2012.

[6] The Auger Collaboration. Pierre Auger Project Design Report. 1997.

[7] Pierre Auger Observatory. Bildersammlung. In *http://augerpc.in2p3.fr/galleries*. October.

[8] Domenico D'Urso. *Pierre Auger Observatory: Fluorescence Detector Event Reconstruction and Data Analysis*. PhD thesis, UNIVERSITA' DEGLI STUDI DI CATANIA.

[9] Marcus Wirtz. Simulation studies of a novel scintillator detector with SiPM readout for muons of cosmic ray air showers. 2014.

[10] T.Abu-Zayyad et. al. A Measurement of the Average Longitudinal Development Profile of Cosmic Ray Air Showers Between $10^{17} eV$and 10^{18}eV. *Astropart.Phys.16:1-11,2001*, 2001.

[11] Fernando Arqueros and Joerg R. Hoerandel and Bianca Keilhauer. Air Fluorescence Relevant for Cosmic-Ray Detection — Summary of the 5th Fluorescence Workshop, El Escorial 2007. *arXiv:0807.3760v1 [astro-ph]*, 2008.

[12] The Pierre Auger Collaboration. The Pierre Auger Observatory: Contributions to the 33rd International Cosmic Ray Conference (ICRC 2013). 2013.

[13] J. Bluemer, R. Engel, and J.R. Hoerandel. Cosmic Rays from the Knee to the Highest Energies. *astro-ph.HE arXiv:0904.0725*, Apr 2009.

[14] The Auger Collaboration. Auger Publications Committee Website. 2014.

[15] J. Abraham et al. The Fluorescence Detector of the Pierre Auger Observatory. *Nucl.Instrum.Meth.*, 2010 / 2009.

[16] C. Meurer and N. Scharf. Heat - a low energy enhancement of the pierre auger observatory. *arXiv:1106.1329 [astro-ph.IM]*, 2011.

[17] T. Niggemann, P. Assis, P. Brogueira, A. Bueno, H.M. Eichler, M. Ferreira, T. Hebbeker, M. Lauscher, L. Mendes, L. Middendorf, S. Navas, C. Peters, M. Pimenta, A. Ruiz, J. Schumacher, M. Stephan. Status of the Silicon Photomultiplier Telescope FAMOUS for the Fluorescence Detection of UHECRs. In *ICRC*, 2013.

[18] Stephan, Maurice, Assis, Pedro, Brogueira, Pedro, Ferreira, Miguel, Hebbeker, Thomas, Lauscher, Markus, Mendes, Luís, Meurer, Christine, Middendorf, Lukas, Pimenta, Mário, and Schumacher, Johannes. Famous - a prototype silicon photomultiplier telescope for the fluorescence detection of ultra-high-energy cosmic rays. *EPJ Web of Conferences*, 53:08015, 2013.

[19] SCHOTT. schott-uv-bandpass-ug11-june-2014-de. *www.schott.com/advanced_optics/german/download/schott-uv-bandpass-ug11-june-2014-de.pdf*, June 2014.

[20] Markus Lauscher, Thomas Hebbeker, Christine Meurer, Tim Niggemann, Johannes Schumacher, Maurice Stephan. Silicon Photomultiplier (SiPM) Characterization for Fluorescence Light Detection. 2011.

[21] Tanguy Pierog and Ralph Engel and Dieter Heck. 3D Air Shower Simulations Using CONEX in CORSIKA. *icrc*, 2009.

[22] Maurice Stephan, Pedro Assis, Pedro Brogueira, Miguel Ferreira, Thomas Hebbeker, Markus Lauscher, Luis Mendes, Christine Meurer, Lukas Middendorf, Mario Pimenta and Johannes Schumacher. FAMOUS – A prototype silicon photomultiplier telescope for the fluorescence detection of ultra-high-energy cosmic rays. In *EPJ Web of Conferences Volume 53, 2013*, 2013.

[23] S. Agostinelli et. al. GEANT4-a simulation toolkit. *Nuclear Instruments and Methods in Physics Research Section A: Accelerators, Spectrometers, Detectors and Associated Equipment*, 2003.

[24] Amit Patel. Hexagonal grids. *http://www.redblobgames.com/grids/hexagons/*, November 2013.

[25] Daniel Kuempel, Karl-Heinz Kampert, Markus Risse. Geometry reconstruction of fluorescence detectors revisite. *Astroparticle Physics*, 2008.

[26] Eugene Antoine Maurice Stephan. *Measurement of the Light Flux of Stars and the Night-Sky with Silicon Photomultipliers*. PhD thesis, RWTH Aachen University , 2014.

Danksagung

An dieser Stelle möchte ich mich bei allen bedanken, die mir diese Arbeit ermöglicht haben und mich dabei unterstützt haben. Zuerst gebührt mein Dank Herrn Prof. Dr. Hebbeker für die Möglichkeit, an diesem Institut meine Arbeit zu schreiben und somit einen Einblicke in die Arbeit einer internationalen Kollaboration und der Software- sowie Hardwareentwicklung eines Fluoreszenz Teleskopes zu erhalten. Besonders bedanke ich mich bei meinem Betreuer Tim Niggemann sowie Christine Peters insbesondere für die Unterstützung bei unzähligen Softwareproblemen und der gesamten Auger Arbeitsgruppe für das freundliche Arbeitsklima. Ausserdem bedanke ich mich herzlich bei meinen beiden Bürokollegen und Freunden Franziska Knuth und Marcus Wirtz für das freundliche Arbeitsklima und die gegenseitige Unterstützung. Zu guter Letzt danke ich meiner Familie und meinen Freunden für ihre Geduld und die Unterstützung, wann immer sie nötig war.

Erklärung

Hiermit versichere ich, dass ich diese Arbeit einschließlich evtl. beigefügter Zeichnungen, Kartenskizzen u.ä.m selbstständig angefertigt und keine anderen als die angegebenen Hilfsmittel und Quellen benutzt habe. Alle Stellen, die dem Wortlaut oder dem Sinn nach anderen Werken entnommen sind, habe ich in jedem einzelnen Fall unter genauer Angabe der Quelle deutlich als Entlehnung kenntlich gemacht.

Aachen, den 10. November 2014

_____

Dominik Sommer